Y-90 PET/MR Imaging optimization with a Bayesian Penalized Likelihood reconstruction algorithm - Supplementary Information

José Calatayud-Jordán[1*], Nuria Carrasco-Vela[2], José Chimeno-Hernández[1], Montserrat Carles-Fariña[3], Consuelo Olivas-Arroyo[1], Pilar Bello-Arqués[1], Daniel Pérez-Enguix[4], Luis Martí-Bonmatí[3,4], Irene Torres-Espallardo[1,3]

[1*]Department of Nuclear Medicine, La Fe University and Polytechnical Hospital, Av. Fernando Abril Martorell 106, Valencia, 46026, Spain.
[2]Radiophysics and Radiological Protection Service, Clinical University Hospital of Valencia, Av. Blasco Ibáñez 17, Valencia, 46010, Spain.
[3]Biomedical Imaging Research Group (GIBI2**30**) at Health Research Institute Hospital La Fe (IIS La Fe), La Fe University and Polytechnical Hospital, Av. Fernando Abril Martorell 106, Valencia, 46026, Spain.
[4]Department of Radiology, La Fe University and Polytechnical Hospital, Av. Fernando Abril Martorell 106, Valencia, 46026, Spain.

*Corresponding author(s). E-mail(s): calatayud_josjor@gva.es;
Contributing authors: carrasco_nur@gva.es; chimeno_jos@gva.es; montserrat_carles@iislafe.es; olivas_con@gva.es; bello_pil@gva.es; perez_daneng1@gva.es; marti_lui@gva.es; torres_ire@gva.es;

S1 Supplementary information

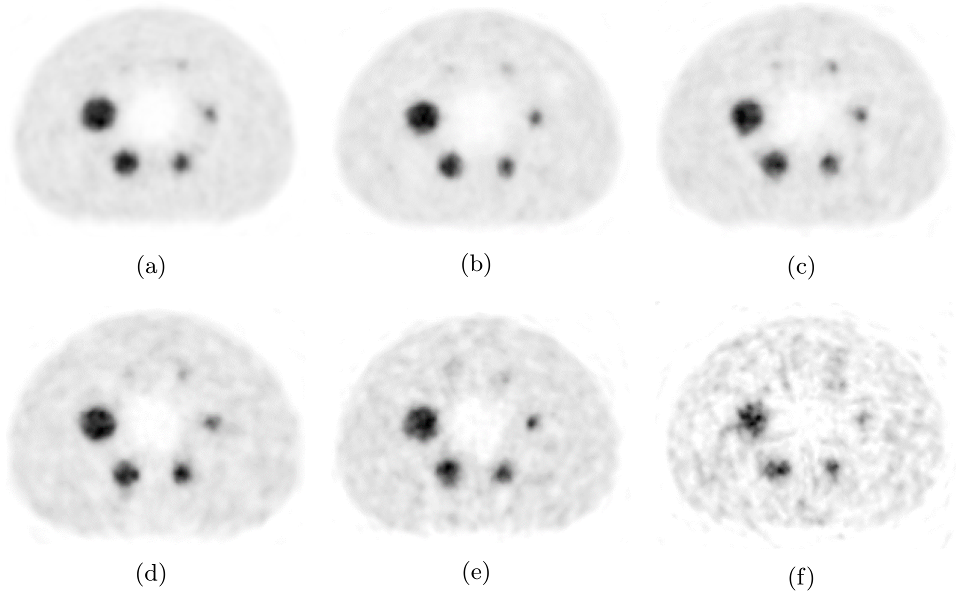

Fig. S1: Transaxial views of the centre of the spheres in the NEMA phantom of PET acquisitions imaged at several times. Phantom activities were: (a) 4.30, (b) 3.30, (c) 2.77, (d) 2.17, (e) 1.61 and (f) 0.922 GBq.

Influence of β parameter

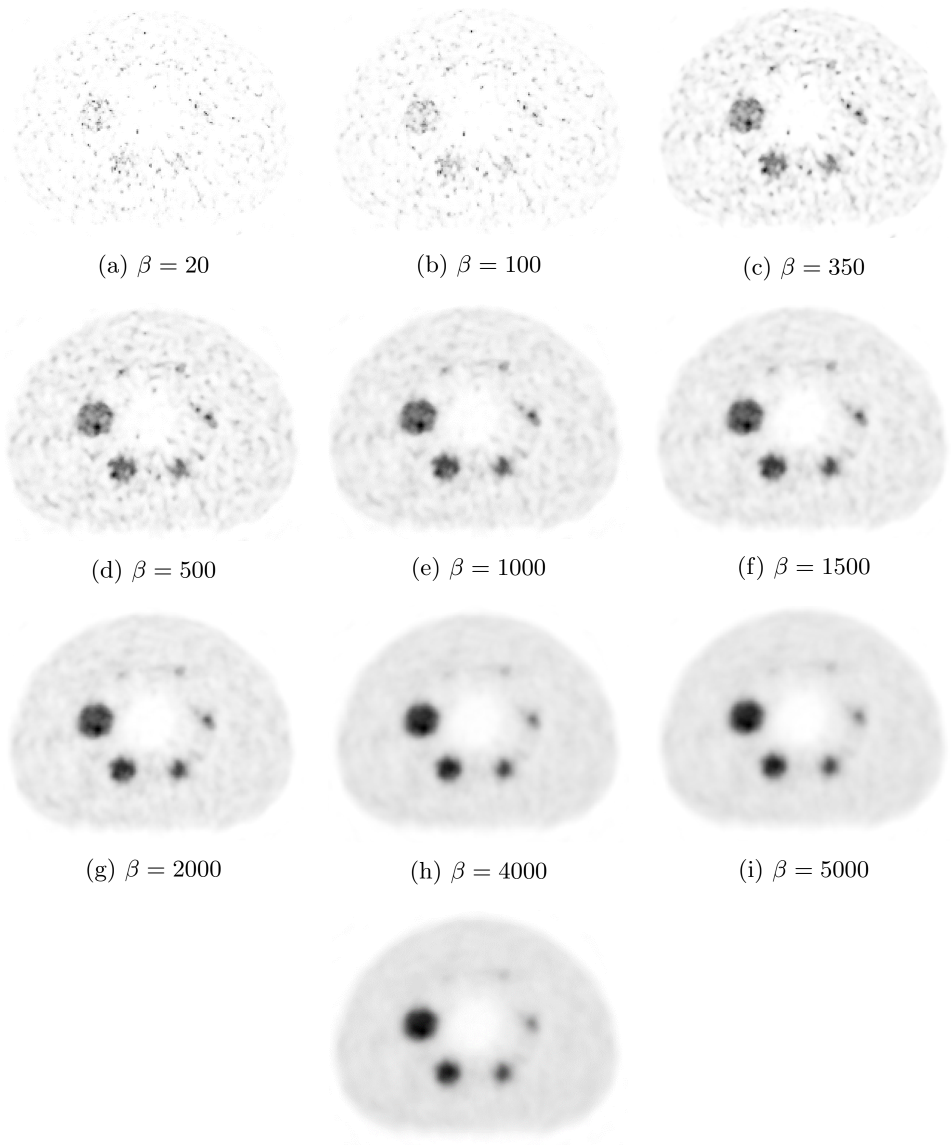

(a) $\beta = 20$ (b) $\beta = 100$ (c) $\beta = 350$

(d) $\beta = 500$ (e) $\beta = 1000$ (f) $\beta = 1500$

(g) $\beta = 2000$ (h) $\beta = 4000$ (i) $\beta = 5000$

(j) $\beta = 6000$

Fig. S2: Transaxial views of the centre of the spheres in the NEMA phantom in the first day of acquisition with an activity of 4.30 GBq and a concentration activity at the hot spheres of 3.30 MBq/ml, with an acquisition time of 20 min. The same scale was used for all images.

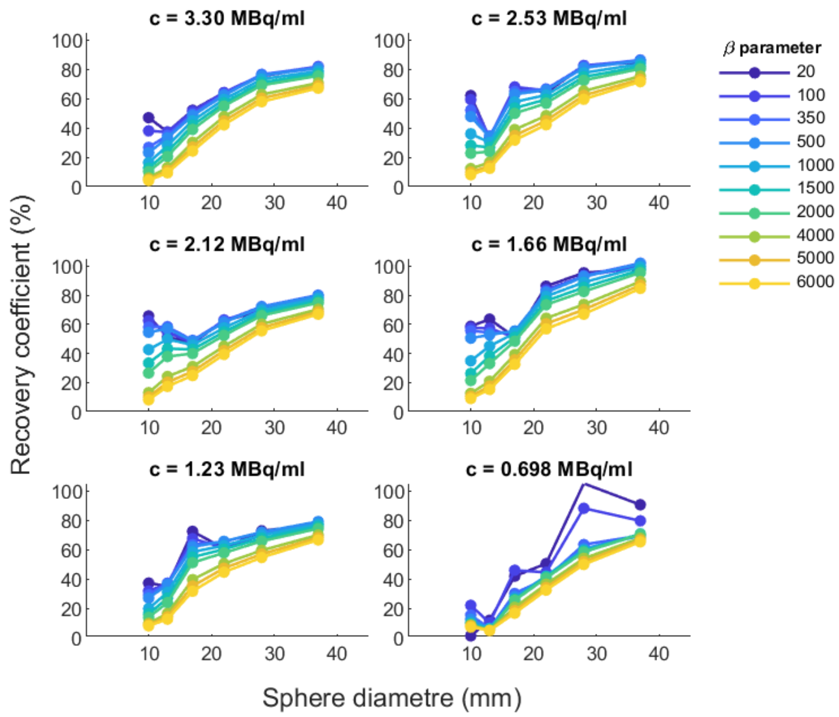

Fig. S3: Recovery coefficients (RC) of NEMA phantom spheres as a function of the diameter for different values of β parameter and activity concentrations.

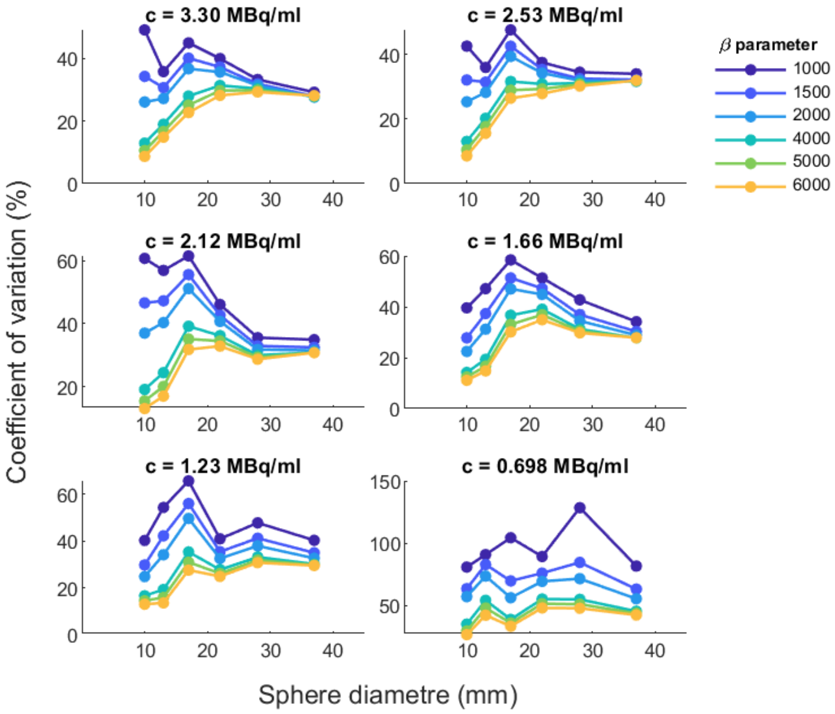

Fig. S4: Coefficient of variation (COV) of NEMA phantom spheres as a function of the diameter for different values of β parameter between 1000 - 6000 and activity concentrations.

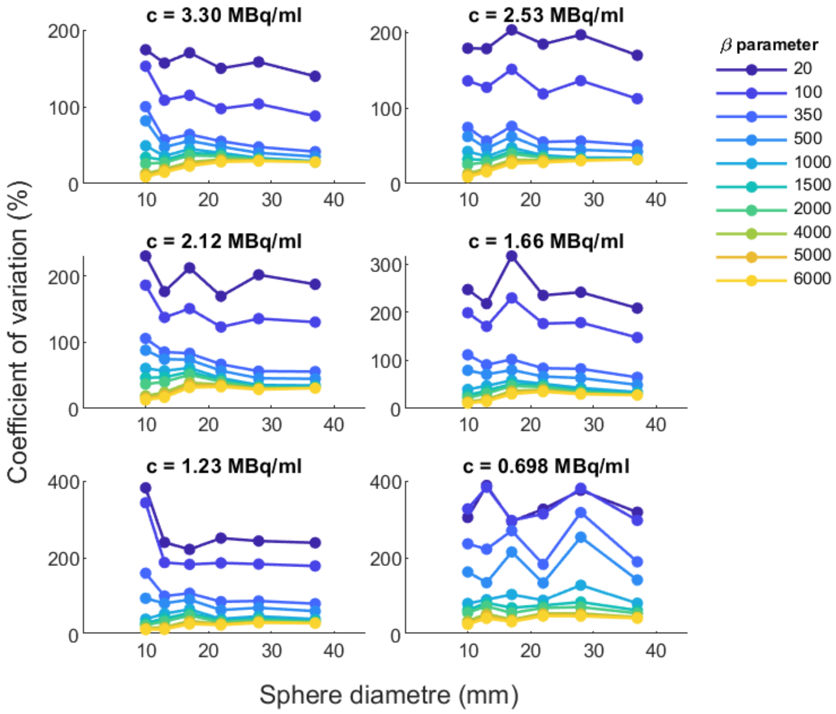

Fig. S5: Coefficient of variation (COV) of NEMA phantom spheres as a function of the diameter for different values of β parameter and activity concentrations.

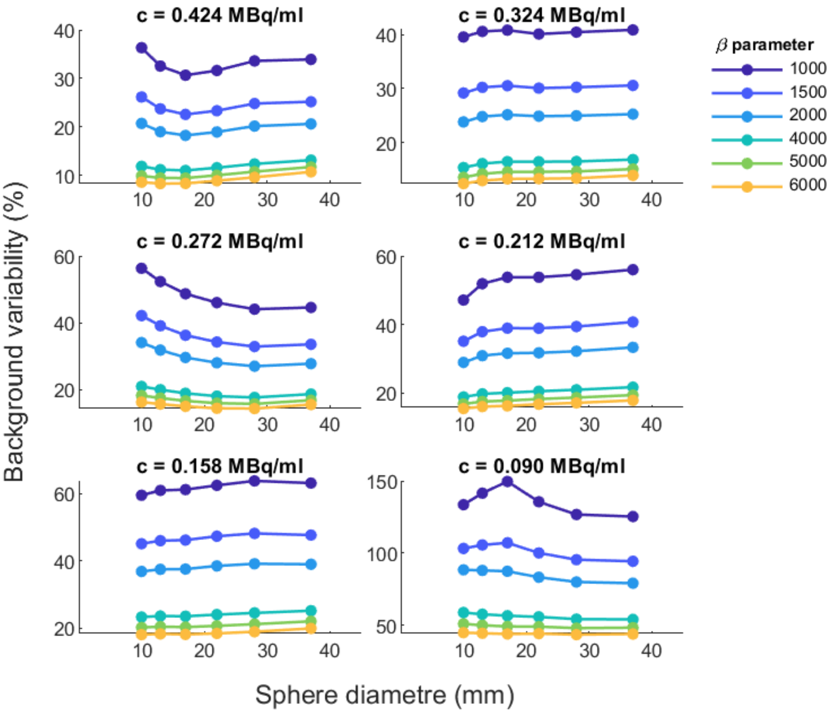

Fig. S6: Background variability (BV) of NEMA phantom as a function of the sphere diameter for different values of β parameter in the 1000 - 6000 range and background activity concentrations.

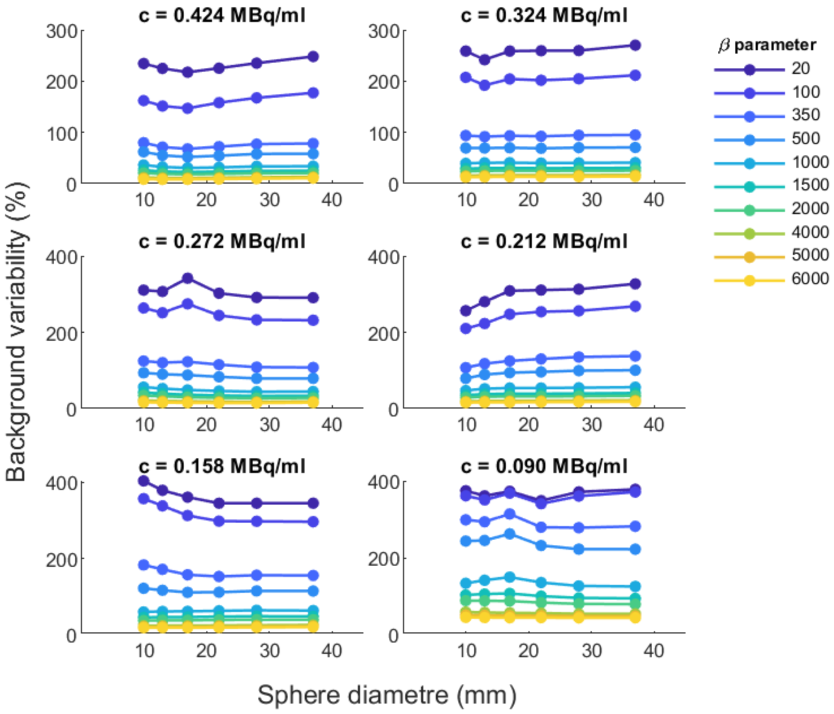

Fig. S7: Background variability (BV) of NEMA phantom as a function of the sphere diameter for different values of β parameter and background activity concentrations.

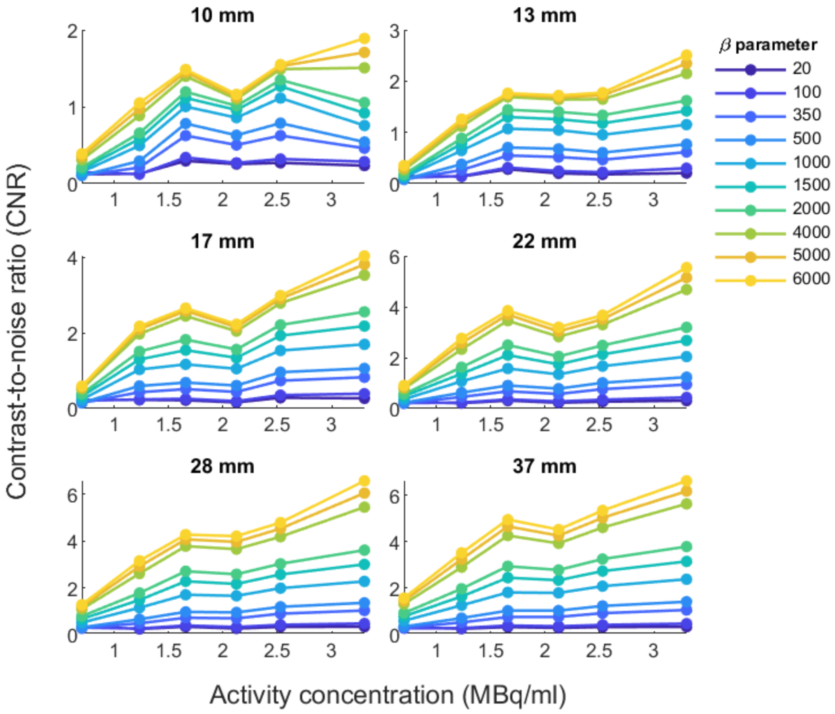

Fig. S8: Contrast-to-noise ratio (CNR) as a function of activity concentration for different sphere diameters and β penalty parameter.

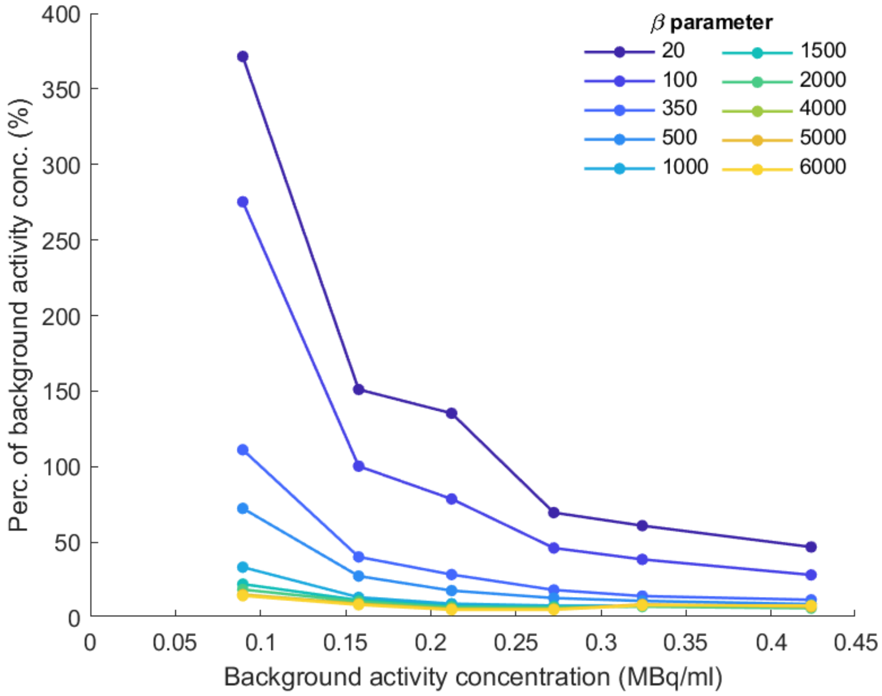

Fig. S9: Percentage of activity concentration from NEMA phantom cold insert as a function of background concentration for different values of β penalty parameter.

Influence of acquisition time

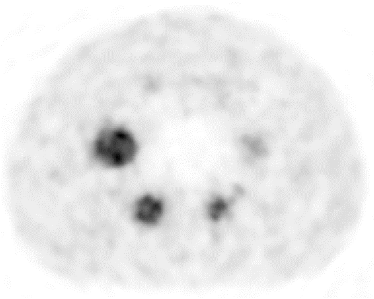

(a) 5 min.

(b) 10 min.

(c) 15 min.

(d) 20 min.

Fig. S10: Transaxial views of PET images at the centre of the spheres in the NEMA phantom in the first day of acquisition, with an activity of 4.30 GBq and a concentration activity at the hot spheres of 3.30 MBq/ml, and reconstructed with Q.Clear using $\beta = 4000$, a matrix size of 384×384, TOF and varying acquisition times.

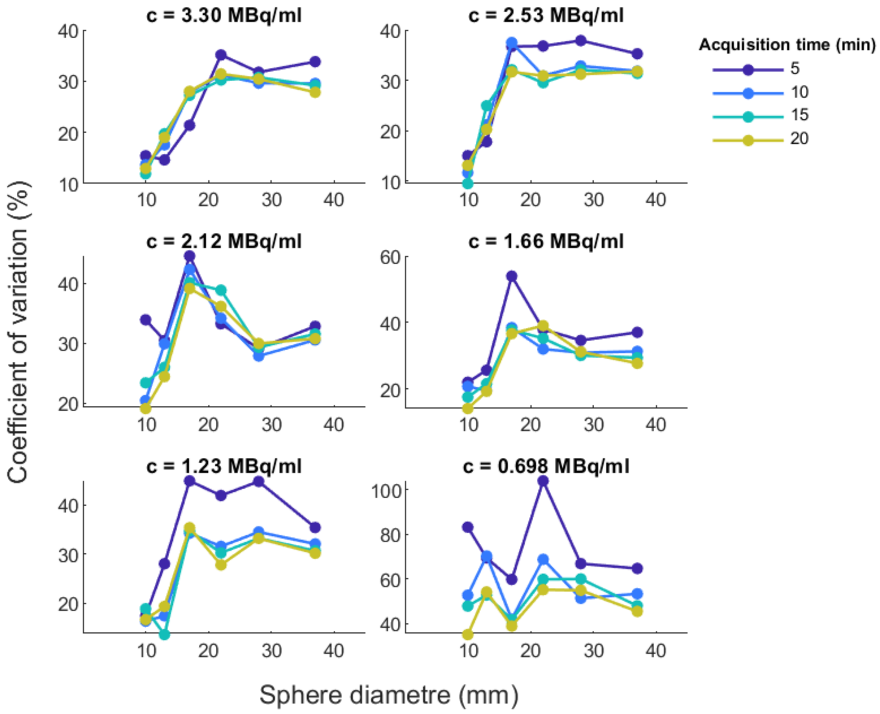

Fig. S11: Coefficient of variation (COV) of NEMA phantom spheres as a function of the diameter for different acquisition times.

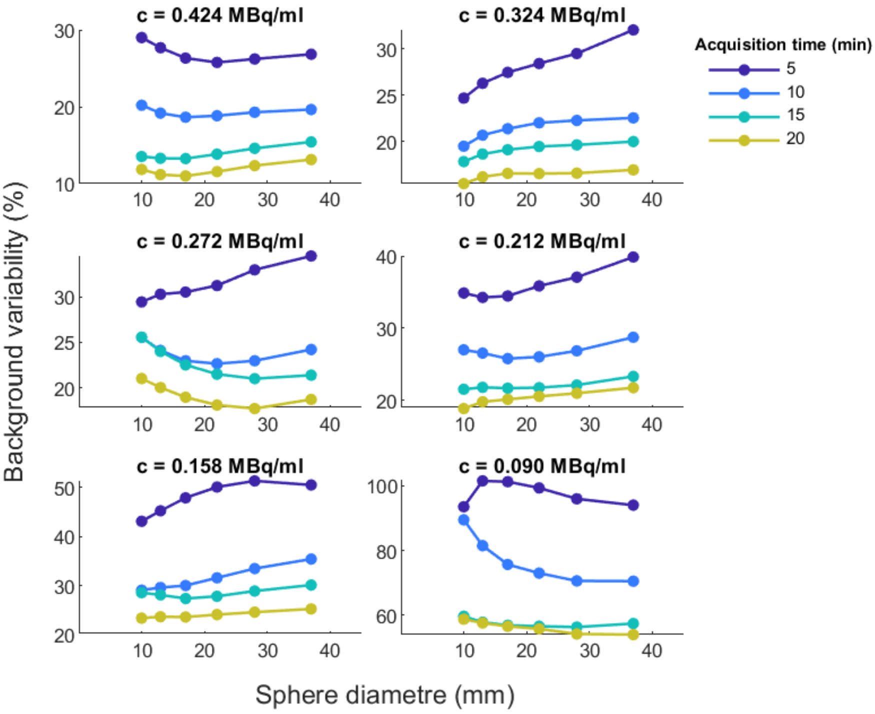

Fig. S12: Background variability (BV) of NEMA phantom as a function of the diameter of the spheres for different acquisition times and activity concentrations.

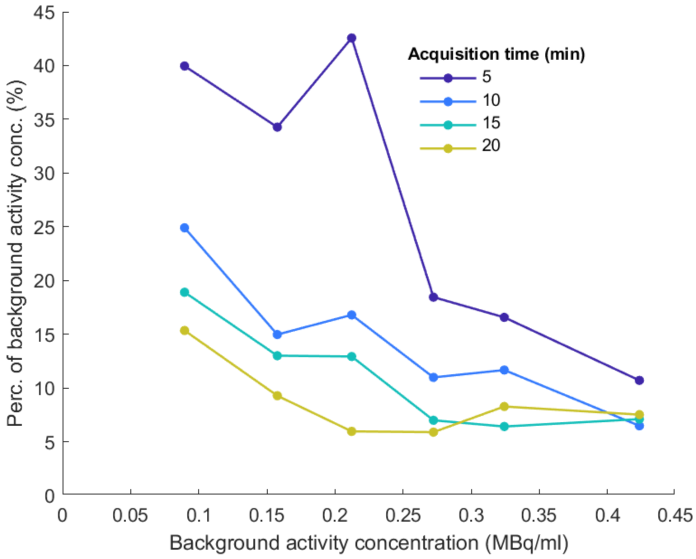

Fig. S13: Percentage of activity concentration from NEMA phantom cold insert as a function of background activity concentration for different acquisition times.

Influence of matrix size

(a) 384 × 384

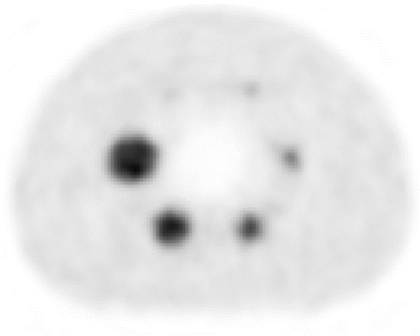

(b) 256 × 256

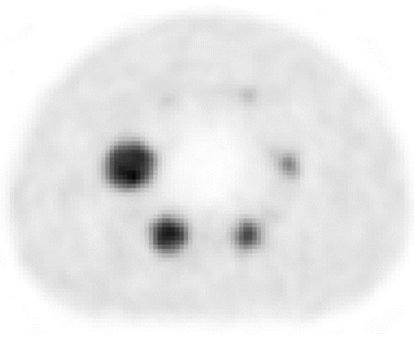

(c) 192 × 192

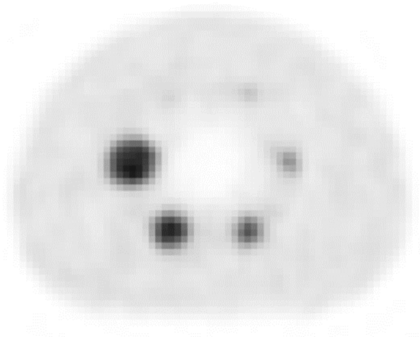

(d) 128 × 128

Fig. S14: Transaxial views of the centre of the spheres in the NEMA phantom in the first day of acquisition, with an activity of 4.30 GBq and a concentration activity at the hot spheres of 3.30 MBq/ml, reconstructed with Q.Clear method using $\beta = 4000$ and TOF, 20 min of acquisition time and varying matrix size. The scale is the same for all images.

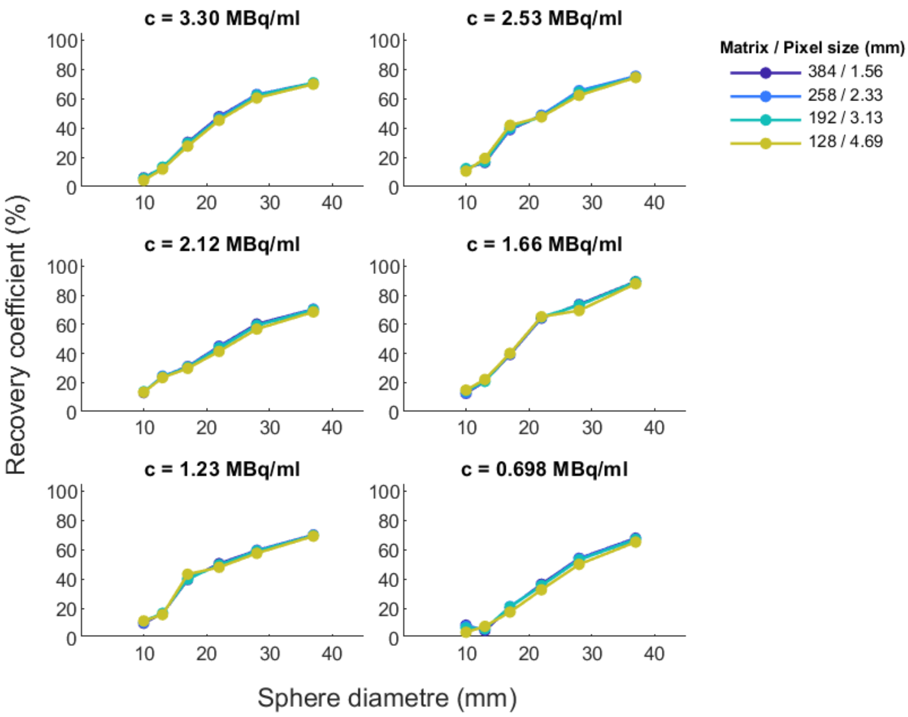

Fig. S15: Recovery coefficients (RC) of NEMA phantom spheres as a function of the diameter for different matrix sizes and activity concentrations.

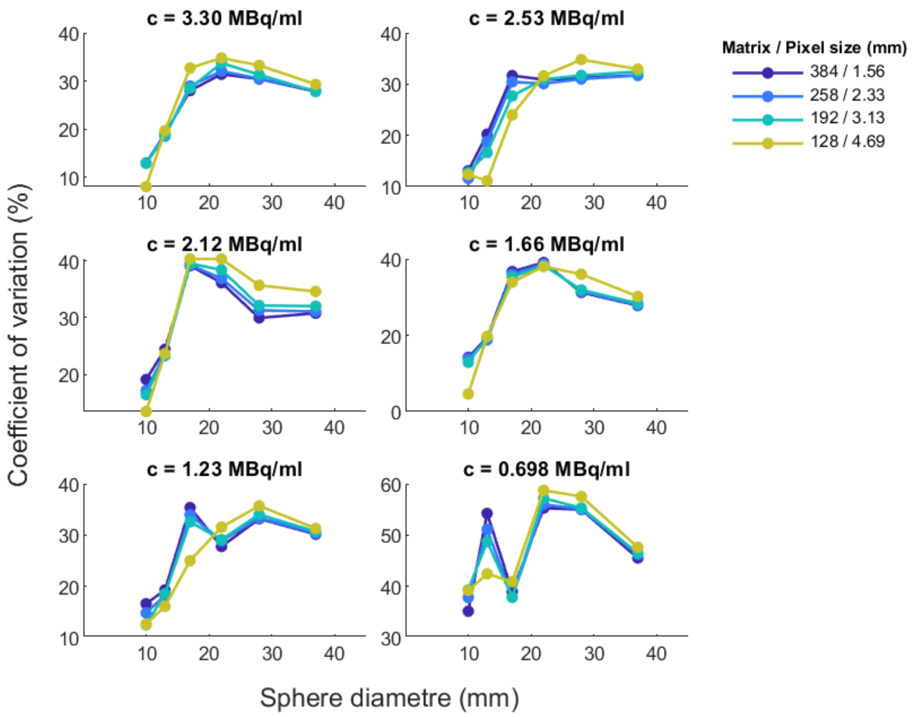

Fig. S16: Coefficient of variation (COV) of NEMA phantom spheres as a function of the diameter for different matrix sizes.

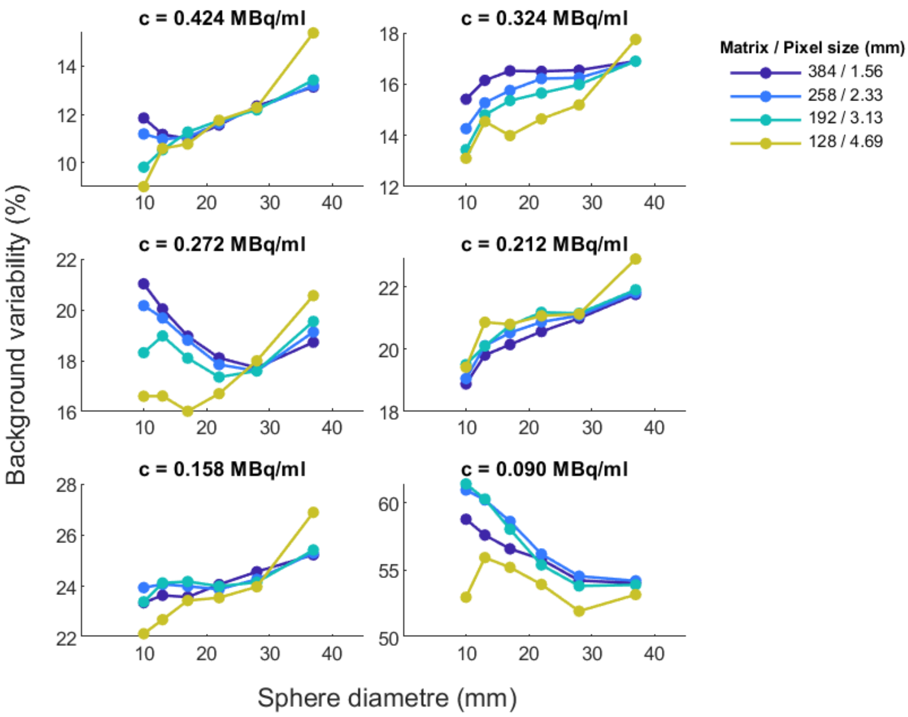

Fig. S17: Background variability (BV) of NEMA phantom as a function of the sphere diameter for different matrix sizes.

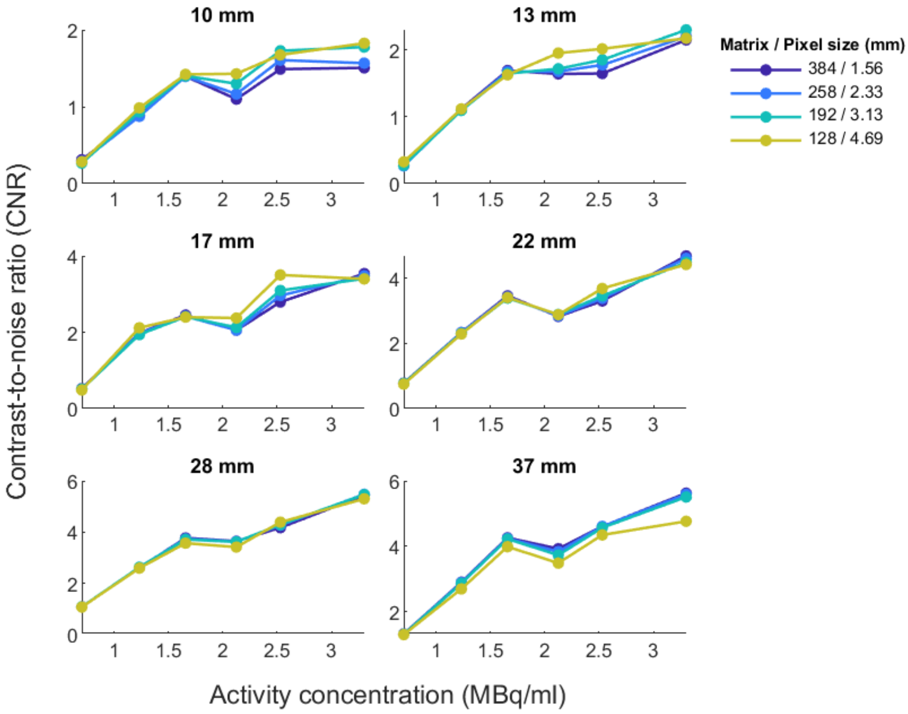

Fig. S18: Contrast-to-noise ratio (CNR) of NEMA phantom spheres for different sphere diameters and matrix size.

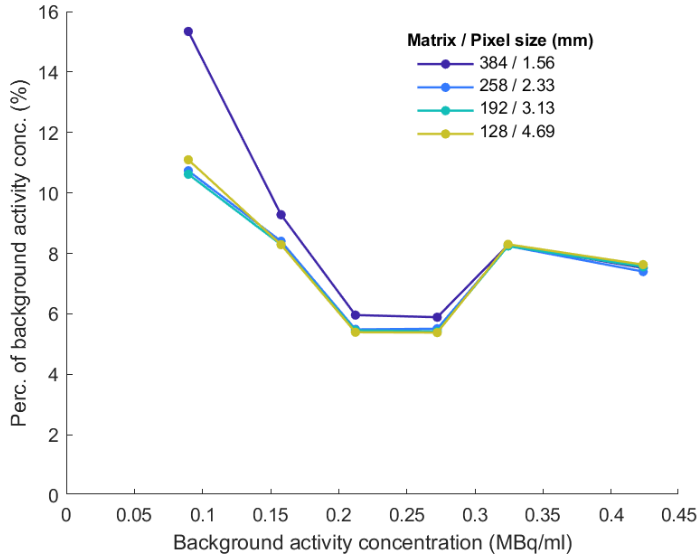

Fig. S19: Percentage of activity concentration of the NEMA phantom cold insert for different background activity concentrations and matrix sizes.

Influence of reconstruction algorithm

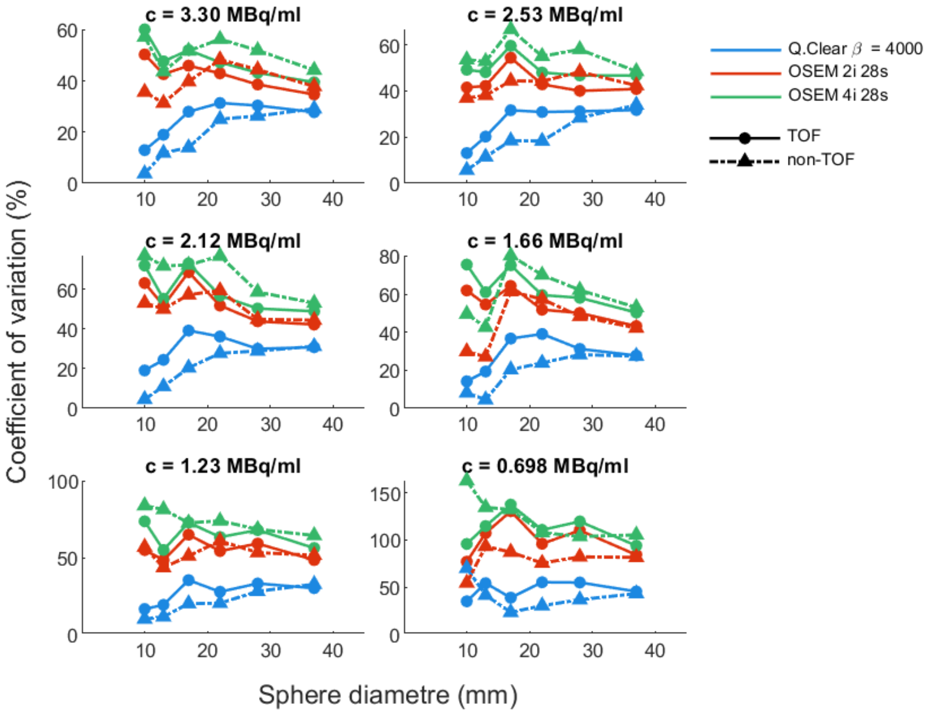

Fig. S20: Coefficient of variation (COV) of NEMA phantom spheres as a function of diameter for different reconstruction and quantification algorithms.

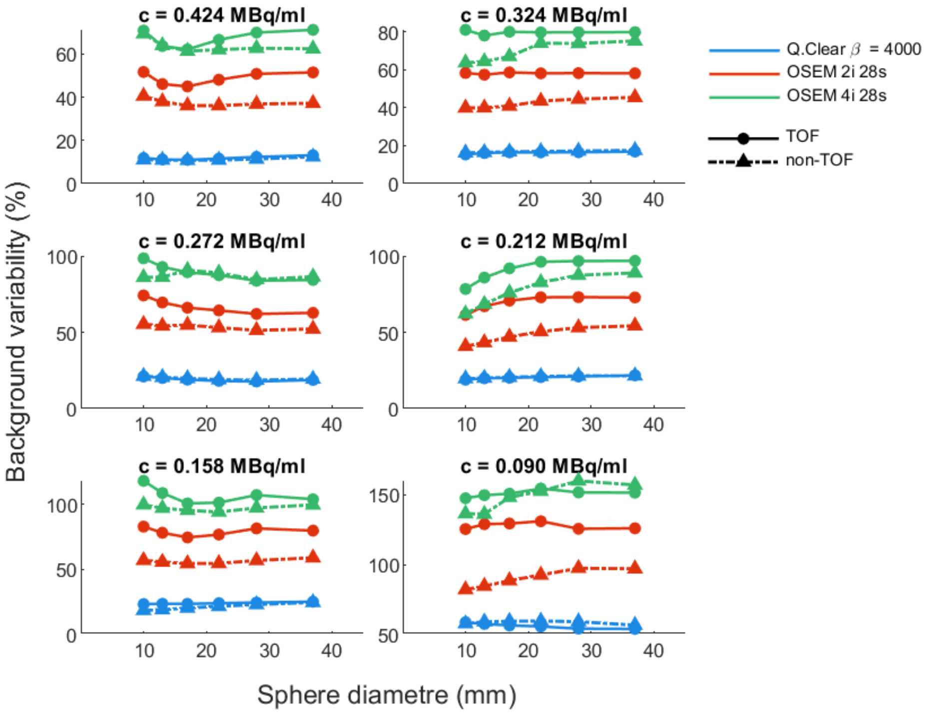

Fig. S21: Background variability (BV) of NEMA phantom as a function of the sphere diameter for different reconstruction and quantification algorithms.

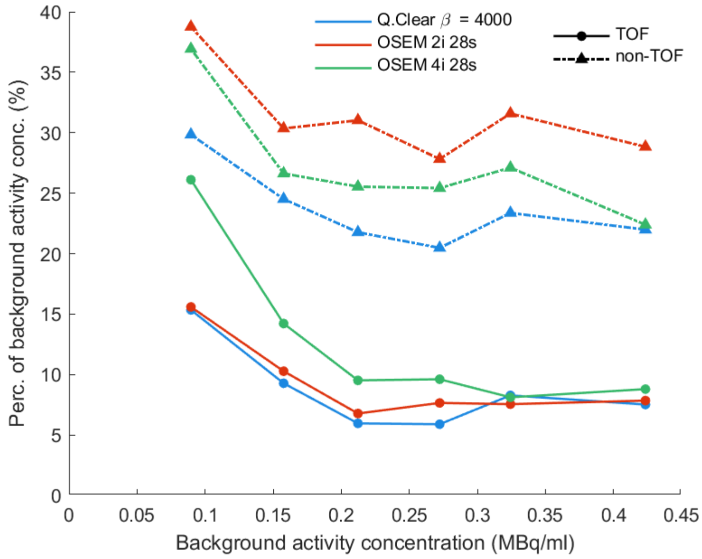

Fig. S22: Percentage of activity concentration of the NEMA phantom cold insert as a function of background activity concentration for different reconstruction and quantification algorithms.